

Quantum Shape-Phase Transitions in Finite Nuclei

A. Leviatan ^{a*}

^aRacah Institute of Physics, The Hebrew University, Jerusalem 91904, Israel

Quantum shape-phase transitions in finite nuclei are considered in the framework of the interacting boson model. Critical-point Hamiltonians for first- and second-order transitions are identified by resolving them into intrinsic and collective parts. Suitable wave functions and finite- N estimates for observables at the critical-points are derived.

1. QUANTUM PHASE TRANSITIONS

Quantum phase transitions are structural changes occurring at zero temperature as a function of a coupling constant and driven by quantum fluctuations. An example is the phase transition between different shapes of nuclei for which the equilibrium deformation plays the role of an order parameter. A proper description of such phase transitions necessitates the inclusion of correlation effects beyond the mean-field level. In a microscopic approach this is done by restoring broken symmetries of the self-consistent mean-field solutions (HFB or HF+BCS) via angular momentum and number projection, and by configuration mixing using the generator coordinate method [1]. Shape-phase transitions in nuclei have also been studied in the geometric framework of a Bohr Hamiltonian for macroscopic quadrupole shapes. Analytic solutions, called E(5) [2] and X(5) [3], were obtained under certain approximations (*e.g.* infinite square-well potentials), and shown to be relevant to nuclei at the critical-points of second- and (low-barrier) first-order transitions respectively [4]. A key issue near criticality is to understand the modifications brought in by the fact that nuclei consist of a finite number of nucleons. This aspect is particularly important for sorting out the phase diagram and structure-evolution of stable and unstable nuclei, as a function of protons and neutrons. In the present contribution we examine this question in the framework of the interacting boson model (IBM) [5] which describes low-lying quadrupole collective states in nuclei in terms of a system of N monopole (s) and quadrupole (d) bosons representing valence nucleon pairs. This algebraic model is simple yet rich enough to encompass the dynamics of quantum shape-phase transitions in nuclei, and illuminate the underlying finite- N structure at the critical-point.

2. GEOMETRY AND CRITICAL-POINT HAMILTONIANS

The starting point for analyzing shapes in the IBM is an energy surface defined by the expectation value of the Hamiltonian in the coherent (intrinsic) state [6, 7]

$$|\beta, \gamma; N\rangle = (N!)^{-1/2} (b_c^\dagger)^N |0\rangle, \quad (1)$$

*This work is supported by the Israel Science Foundation.

where $b_c^\dagger = (1 + \beta^2)^{-1/2}[\beta \cos \gamma d_0^\dagger + \beta \sin \gamma (d_2^\dagger + d_{-2}^\dagger)/\sqrt{2} + s^\dagger]$. For the general IBM Hamiltonian with one- and two-body interactions, the energy surface takes the form

$$E_N(\beta, \gamma) = E_0 + N(N-1) [a\beta^2 - b\beta^3 \cos 3\gamma + c\beta^4] (1 + \beta^2)^{-2}. \quad (2)$$

The coefficients E_0, a, b, c involve particular linear combinations of the Hamiltonian's parameters [8, 9]. The equilibrium shape for a given Hamiltonian is determined by the global minimum, $(\beta_{eq}, \gamma_{eq})$, of the energy surface, and can be spherical ($\beta_{eq} = 0$) or deformed ($\beta_{eq} > 0$) with prolate ($b > 0$), oblate ($b < 0$) and γ -independent ($b = 0$) character. For $\beta > 0$ the intrinsic state of Eq. (1) is deformed, and represents a band whose rotational members are obtained by projection. For example, for $\gamma = 0$ the band consists of states with good $O(3)$ symmetry $L = 0, 2, 4, \dots, 2N$, given by

$$|\beta; N, L, M\rangle \propto \hat{\mathcal{P}}_{LM}|\beta, \gamma = 0; N\rangle. \quad (3)$$

The projected states with fixed N and L , involve a mixture of components $|N, n_d, \tau, L\rangle$ with quantum numbers related to the $U(6) \supset U(5) \supset O(5) \supset O(3)$ chain. For $\beta = 0$ one recovers the $U(5)$ spherical ground state, $|s^N\rangle \equiv |N, n_d = \tau = L = 0\rangle$. When the deformed shape is γ -independent, a projection on $O(5)$ symmetry τ is required

$$|\beta; N, \tau, L, M\rangle \propto \hat{\mathcal{P}}_{\tau, LM}|\beta, \gamma; N\rangle. \quad (4)$$

Stable shapes are characterized by a deep well-localized single minimum in the energy surface. In this case, the projection after variation procedure mentioned above provides an accurate approximation to members of the ground band. The dynamical symmetry limits of the IBM are examples of such stable structures, corresponding to a $U(5)$ spherical vibrator ($\beta_{eq} = 0$), $SU(3)$ deformed-rotor [$(\beta_{eq} = \sqrt{2}, \gamma_{eq} = 0)$] and an $O(6)$ γ -independent rotor ($\beta_{eq} = 1$). At a phase transition the energy surface serves as a Landau's potential and displays a different topology. In a first-order phase transition it has two coexisting minima which become degenerate at the critical-point. In a second-order phase transition the energy surface changes continuously from one minimum to another, becoming flat-bottomed at the critical-point. Typical examples are shown in Fig. 1. The corresponding conditions on the energy surface at the critical-points are

$$\begin{aligned} 1^{st} \text{ order} \quad & b^2 = 4ac, \quad a > 0, \quad b \neq 0 \\ 2^{nd} \text{ order} \quad & a = 0, \quad b = 0, \quad c > 0. \end{aligned} \quad (5)$$

Phase transitions for finite N can be studied in the IBM by an Hamiltonian of the form, $H_1 + gH_2$, involving terms from different dynamical symmetry chains [7]. The critical value of the control parameter g_c is determined by the corresponding condition in Eq. (5). Several studies of this type have identified a $U(5)$ - $SU(3)$ first-order transition with an extremely low-barrier, a $U(5)$ - $O(6)$ second-order transition, and a $O(6)$ - $SU(3)$ cross-over [7, 10]. To consider shape-phase transitions of a general character, without being restricted to a particular form for the Hamiltonian, it is convenient to resolve the critical-Hamiltonian into intrinsic and collective parts [8, 9],

$$H_{cri} = H_{int} + H_c. \quad (6)$$

The intrinsic part (H_{int}) is defined to have the equilibrium condensate $|\beta = \beta_{eq}, \gamma_{eq}; N\rangle$,

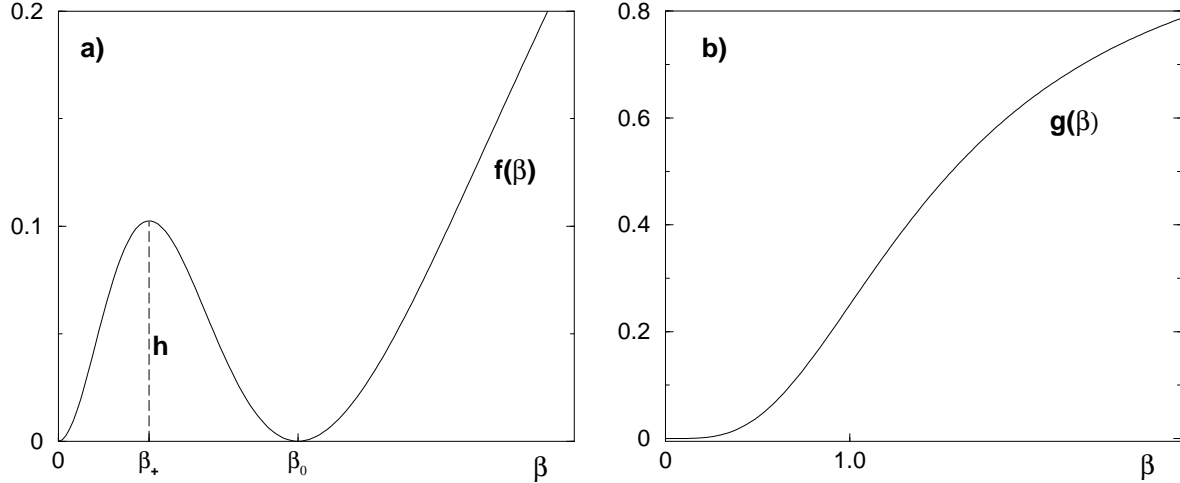


Figure 1. Energy surfaces at the critical-points. (a) First-order transition, Eq. (8). (b) Second-order transition, Eq. (14). Asymptotically, $f(\infty) = g(\infty) = 1$.

Eq. (1), as an exact zero-energy eigenstate and to have an energy surface with the same shape as the critical energy surface. The collective part (H_c) is composed of kinetic terms which do not affect the shape of the energy surface, and can be transcribed in the form

$$H_c = c_3 \left[\hat{C}_{O(3)} - 6\hat{n}_d \right] + c_5 \left[\hat{C}_{O(5)} - 4\hat{n}_d \right] + c_6 \left[\hat{C}_{\overline{O(6)}} - 5\hat{N} \right] + E_0 . \quad (7)$$

Here $\hat{N} = \hat{n}_d + \hat{n}_s$, \hat{n}_d and \hat{n}_s are the total-boson, d -boson and s -boson number operators respectively. \hat{C}_G denotes the quadratic Casimir operator of the group G as defined in [9]. The intrinsic-collective resolution constitutes an efficient method for studying shape-phase transitions, since the derived Hamiltonian is tailored to reproduce a given energy surface which, in-turn, governs the nature of the phase transition.

3. FIRST-ORDER CRITICAL-POINT

The energy surface at the critical-point of a first-order transition between spherical and prolate-deformed shapes has the following form for $\gamma = 0$

$$E_{cri}(\beta) = E_0 + c N(N-1) f(\beta) , \quad f(\beta) = \beta^2 (1 + \beta^2)^{-2} (\beta - \beta_0)^2 . \quad (8)$$

As shown in Fig. 1(a), $E_{cri}(\beta)$ has two degenerate minima at $\beta = 0$ and $\beta = \beta_0 = 2a/b = b/2c > 0$. The value of β_0 controls the position, $\beta = \beta_+ = (-1 + \sqrt{1 + \beta_0^2})/\beta_0$, and height $h = f(\beta_+) = (-1 + \sqrt{1 + \beta_0^2})^2/4$ of the barrier. In this case, the intrinsic part (H_{int}) has the equilibrium condensate $|\beta = \beta_0, \gamma = 0; N\rangle$, Eq. (1), as an exact zero-energy eigenstate and has an energy surface as in Eq. (8) (with $E_0 = 0$). H_{int} has the form [11]

$$H_{int} = h_2 P_2^\dagger(\beta_0) \cdot \tilde{P}_2(\beta_0) , \quad P_{2\mu}^\dagger(\beta_0) = \beta_0 s^\dagger d_\mu^\dagger + \sqrt{7/2} \left(d^\dagger d^\dagger \right)_\mu^{(2)} , \quad (9)$$

with $\tilde{P}_{2\mu}(\beta_0) = (-1)^\mu P_{2,-\mu}(\beta_0)$ and $h_2 = c$. By construction H_{int} is rotational-scalar and has the L -projected states $|\beta = \beta_0; N, L\rangle$ of Eq. (3) as solvable deformed eigenstates with

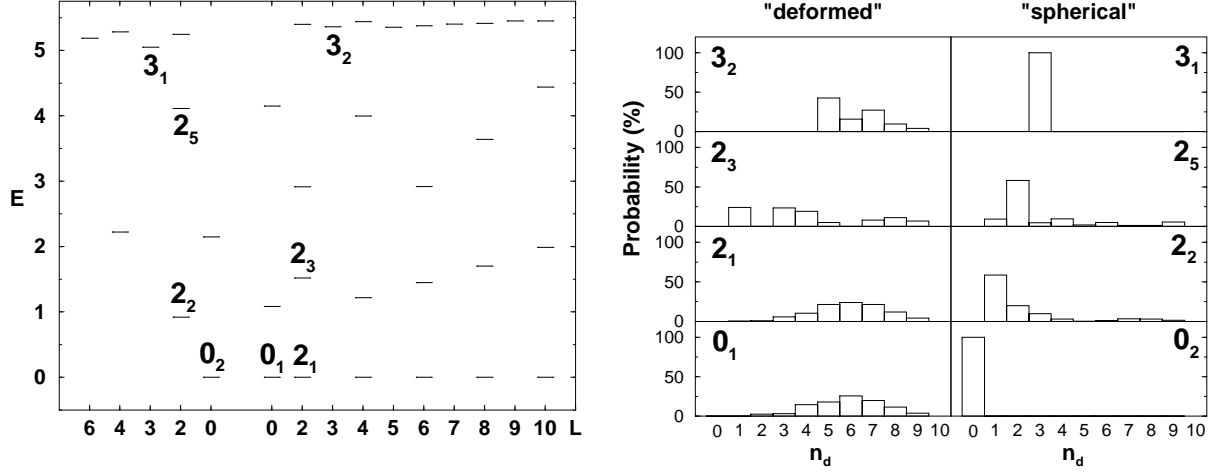


Figure 2. Left: spectrum of H_{int} , Eq. (9), with $h_2 = 0.1$, $\beta_0 = 1.3$ and $N = 10$. Right: the number of d bosons (n_d) probability distribution for selected eigenstates of H_{int} .

energy $E = 0$. It has also solvable spherical eigenstates: $|N, n_d = \tau = L = 0\rangle \equiv |s^N\rangle$ and $|N, n_d = \tau = L = 3\rangle$ with energy $E = 0$ and $E = 3h_2[\beta_0^2(N-3) + 5]$ respectively. Accordingly, the exact spectrum of H_{int} shown in Fig. 2, displays a zero-energy deformed ($K = 0$) ground band, degenerate with a spherical ($n_d = 0$) ground state. The remaining states are either predominantly spherical, or deformed states arranged in several excited $K = 0$ bands below the γ band. The coexistence of spherical and deformed states is evident in the right portion of Fig. 2, which shows the n_d decomposition of wave functions of selected eigenstates of H_{int} . The “deformed” states show a broad n_d distribution typical of a deformed rotor structure. The “spherical” states show the characteristic dominance of single n_d components that one would expect for a spherical vibrator. Table 1 shows the effect of different rotational terms in H_c , Eq. (7). For a high-barrier ($\beta_0 = 1.3$, $h = 0.1$), the calculated spectrum resembles a rigid-rotor ($E \sim a_N L(L+1)$) for the c_3 -term, a rotor with centrifugal stretching ($E \sim a_N L(L+1) - b_N[L(L+1)]^2$) for the c_5 -term, and a $X(5)$ -like spectrum for the c_6 -term. In all cases the $B(E2)$ values are close to the rigid-rotor Alaga values. Insight of the underlying structure at the critical-point can be gained by examining the L -projected energy surface, obtained by the matrix element of the critical Hamiltonian (6) in the states (3), $E_L^{(N)}(\beta) = \langle \beta; N, L | H_{cri} | \beta; N, L \rangle = \tilde{E}_L^{(N)}(\beta) + E_0$,

$$\begin{aligned} \tilde{E}_L^{(N)}(\beta) = & h_2(\beta - \beta_0)^2 \Sigma_{2,L}^{(N)} + c_3 [L(L+1) - 6D_{1,L}^{(N)}] + c_5 [D_{2,L}^{(N)} - \beta^4 S_{2,L}^{(N)}] \\ & + c_6 [N(N-1) - (1 + \beta^2)^2 S_{2,L}^{(N)}] . \end{aligned} \quad (10)$$

Here $D_{1,L}^{(N)}$, $S_{2,L}^{(N)}$, $D_{2,L}^{(N)}$ and $\Sigma_{2,L}^{(N)}$ denote the expectation values in the states $|\beta; N, L\rangle$ of \hat{n}_d , $\hat{n}_s(\hat{n}_s - 1)$, $\hat{n}_d(\hat{n}_d - 1)$ and $\hat{n}_s\hat{n}_d$ respectively. The mixing between the coexisting spherical and deformed $L = 0$ states, $|\phi_1\rangle \equiv |s^N\rangle$ and $|\phi_2\rangle \equiv |\beta; N, L = 0\rangle$, can be studied by transforming to an orthonormal basis

$$\begin{aligned} |\Psi_1\rangle &= |\phi_1\rangle , \quad |\Psi_2\rangle = (1 - r_{12}^2)^{-1/2} (|\phi_2\rangle - r_{12}|\phi_1\rangle) , \\ r_{12} &= \langle\phi_1|\phi_2\rangle , \end{aligned} \quad (11)$$

Table 1

Excitation energies (in units of $E(2_1^+) = 1$) and B(E2) values [in units of $B(E2; 2_1^+ \rightarrow 0_1^+ = 1)$] for first-order critical-point Hamiltonians [high barrier: Eqs. (6),(7),(9), low barrier: Eq. (13)], with $N = 10$. The entries in square brackets [...] are estimates based on the L -projected states, Eq. (3), with values of β determined by the global minimum of the respective lowest eigenvalue of the potential matrix, Eqs. (12). The rigid-rotor and X(5) [3] predictions are shown for comparison. Adapted from [11, 12].

	high-barrier ($\beta_0 = 1.3, h = 0.1$)			low-barrier	rotor	X(5)
	$c_3/h_2 = 0.05$	$c_5/h_2 = 0.1$	$c_6/h_2 = 0.05$	$\epsilon/\kappa = 38.25$		
$E(4_1^+)$	3.32 [3.32]	3.28 [3.28]	2.81 [2.87]	2.43 [2.46]	3.33	2.91
$E(6_1^+)$	6.98 [6.97]	6.74 [6.76]	5.43 [5.63]	4.29 [4.33]	7.00	5.45
$E(8_1^+)$	11.95 [11.95]	11.23 [11.29]	8.66 [9.04]	6.53 [6.56]	12.00	8.51
$E(10_1^+)$	18.26 [18.26]	16.58 [16.69]	12.23 [12.83]	9.12 [9.13]	18.33	12.07
$E(0_2^+)$	6.31 [6.30]	6.01 [5.93]	4.56 [5.03]	2.64 [3.30]		5.67
$4_1^+ \rightarrow 2_1^+$	1.40 [1.40]	1.40 [1.40]	1.46 [1.45]	1.61 [1.60]	1.43	1.58
$6_1^+ \rightarrow 4_1^+$	1.48 [1.48]	1.48 [1.48]	1.55 [1.53]	1.85 [1.80]	1.57	1.98
$8_1^+ \rightarrow 6_1^+$	1.45 [1.45]	1.45 [1.45]	1.53 [1.51]	1.92 [1.87]	1.65	2.27
$10_1^+ \rightarrow 8_1^+$	1.37 [1.37]	1.37 [1.37]	1.44 [1.42]	1.87 [1.86]	1.69	2.61
$0_2^+ \rightarrow 2_1^+$	0.003 [0.003]	0.003 [0.004]	0.24 [0.18]	0.78 [0.61]		0.63

and examining the 2×2 potential energy matrix, $K_{ij}(\beta) = \langle \Psi_i | H_{cri} | \Psi_j \rangle$, which reads

$$\begin{aligned} K_{11}(\beta) &= E_0 , \quad K_{12}(\beta) = -c_6 \beta^2 N(N-1)(1-r_{12}^2)^{-1/2} r_{12} , \\ K_{22}(\beta) &= \left[\tilde{E}_{L=0}^{(N)}(\beta) + 2c_6 \beta^2 N(N-1) r_{12}^2 \right] (1-r_{12}^2)^{-1} + E_0 . \end{aligned} \quad (12)$$

The derived eigenvalues of the matrix serve as eigenpotentials, $E_{L=0}^{(\pm)}(\beta)$, and the corresponding eigenvectors, $|\Phi_{L=0}^{(\pm)}\rangle$, are identified with the ground (0_1^+) and excited (0_i^+) $L = 0$ states. The deformed states $|\beta; N, L\rangle$ of Eq. (3) with $L > 0$ are identified with excited members of the ground-band (L_1^+) with energies given by $E_L^{(N)}(\beta)$, Eq. (10). B(E2) values between these states can also be evaluated in closed form [11, 12]. The parameter β in the indicated wave functions and matrix elements is chosen at the global minimum of the lowest eigenvalue, $E_{L=0}^{(-)}(\beta)$, of the matrix $K_{ij}(\beta)$ (12). As is evident from Table 1, this procedure leads to accurate finite- N estimates of observables at the critical-point. The characteristic spectra, discussed above, of the rotational terms in H_c (7) can now be understood from the L -dependence of their respective contributions to $E_L^{(N)}(\beta)$, Eq. (10), and $K_{ij}(\beta)$, Eq. (12). All rotational terms contribute diagonal $L(L+1)$ -type splitting. The c_6 -term controls the mixing which is essential for obtaining an $X(5)$ -like spectrum.

The same type of analysis can be done [12] for a first-order critical-point with a low barrier. A representative Hamiltonian for this class is the critical $U(5)-SU(3)$ Hamiltonian

$$H_{cri} = \epsilon \hat{n}_d - \kappa Q \cdot Q , \quad \epsilon = 9\kappa(2N-3)/4 . \quad (13)$$

Its intrinsic and collective resolution corresponds to the choice $h_2 = 4\kappa$, $\beta_0 = 1/2\sqrt{2}$, $c_3 = 15\kappa/8$, $c_5 = -9\kappa/2$, $c_6 = \kappa$, $E_0 = -5\kappa N$ in Eqs. (7),(9). The resulting barrier is

extremely low, $h \approx 10^{-3}$. The spectrum and E2 rates, shown in Table 1, resemble the X(5) predictions albeit finite-N modifications.

4. SECOND-ORDER CRITICAL-POINT

The energy surface for a second-order transition between spherical and γ -unstable deformed shapes is independent of γ and has the following form at the critical-point

$$E_{cri}(\beta) = E_0 + c N(N-1)g(\beta) , \quad g(\beta) = \beta^4 (1 + \beta^2)^{-2} . \quad (14)$$

As shown in Fig 1(b), $E_{cri}(\beta)$ exhibits a flat-bottomed behavior ($\sim \beta^4$) for small β , hence the single minimum at $\beta = 0$ is not well-localized and experiences large β fluctuations. The relevant critical Hamiltonian (6) has $O(5)$ symmetry. Its intrinsic part is given by

$$H_{int} = t_0 \hat{n}_d(\hat{n}_d - 1) , \quad (15)$$

with $t_0 = c$, and the collective part has the form given in Eq. (7). The states $|\beta; N, \tau, L\rangle$ of Eq. (4) constitute suitable wave functions for yrast states at the critical-point, with the value of β chosen at the global minimum of the $O(5)$ -projected energy surface, $E_{\tau, L}^{(N)}(\beta) = \langle \beta; N, \tau, L | H_{cri} | \beta; N, \tau, L \rangle$,

$$E_{\tau, L}^{(N)}(\beta) = t_0 D_{2, \tau}^{(N)} + c_3 \left[L(L+1) - 6D_{1, \tau}^{(N)} \right] + c_5 \left[\tau(\tau+3) - 4D_{1, \tau}^{(N)} \right] + c_6 \left[N(N-1) - (1 + \beta^2)^2 S_{2, \tau}^{(N)} \right] + E_0 . \quad (16)$$

Here $D_{1, \tau}^{(N)}$, $D_{2, \tau}^{(N)}$ and $S_{2, \tau}^{(N)}$ denote the expectation values in the states $|\beta; N, \tau, L\rangle$ of \hat{n}_d , $\hat{n}_d(\hat{n}_d - 1)$ and $\hat{n}_s(\hat{n}_s - 1)$ respectively. This procedure has been tested in [13] for a representative Hamiltonian of this class, namely, the $U(5)$ - $O(6)$ critical Hamiltonian, $H_{cri} = \epsilon \hat{n}_d + A \hat{P}_6$, with $\epsilon = (N-1)A$. Its intrinsic-collective resolution corresponds to the choice $t_0 = A$, $c_3 = 0$, $c_5 = -A/2$, $c_6 = A/4$, $E_0 = AN(N-1)/4$. in Eqs. (7),(15).

REFERENCES

1. M. Bender, P. H. Heenen and P.G. Reinhard, Rev. Mod. Phys. 75 (2003) 121.
2. F. Iachello, Phys. Rev. Lett. 85 (2000) 3580.
3. F. Iachello, Phys. Rev. Lett. 87 (2001) 052502.
4. R. F. Casten and N. V. Zamfir, Phys. Rev. Lett. 85 (2000) 3584; 87 (2001) 052503.
5. F. Iachello and A. Arima, The Interacting Boson Model, Cambridge Univ. Press, Cambridge 1987.
6. J. N. Ginocchio and M. W. Kirson, Phys. Rev. Lett. 44 (1980) 1744.
7. A. E. L. Dieperink, O. Scholten and F. Iachello, Phys. Rev. Lett. 44 (1980) 1747.
8. M. W. Kirson and A. Leviatan, Phys. Rev. Lett. 55 (1985) 2846.
9. A. Leviatan, Ann. Phys. (NY) 179 (1987) 201.
10. F. Iachello and N. V. Zamfir, Phys. Rev. Lett. 92 (2004) 212501 and references therein.
11. A. Leviatan, (2006) submitted for publication.
12. A. Leviatan, Phys. Rev. C 72 (2005) 031305.
13. A. Leviatan and J. N. Ginocchio, Phys. Rev. Lett. 90 (2003) 212501.